Effect of Low Temperature on Fatigue Crack Propagation Rates of DH36 Steel and Its Butt Weld

Weidong Zhao
Tel: +86-188-4613-6841
E-mail address: zwd_ship@hrbeu.edu.cn
Institution: Harbin Engineering University

Guoqing Feng*(Corresponding author)
Tel: +86-137-6688-9102
E-mail address: fengguoqing@hrbeu.edu.cn
Institution: Harbin Engineering University

Ming Zhang
Tel: +86-157-0461-9178
E-mail address: zhangmingai123@hrbeu.edu.cn
Institution: Harbin Engineering University

Huilong Ren
Tel: +86-135-0451-9650
E-mail address: renhuilong@263.net
Institution: Harbin Engineering University

Chana Sinsabvarodom
Tel: +47-7355-9414
E-mail address: chana.sinsabvarodom@ntnu.no
Institution: Norwegian University of Science and Technology

Abstract： As common marine steel for polar ships, the fatigue crack propagation rates of DH36 steel at low temperature have a crucial influence on the evaluation of the fatigue strength of polar ships. The purpose of this paper is to study the fatigue crack propagation rates of DH36 steel with the different scenarios between the conventional base metal and butt weld specimens at room temperature (RT) and -60℃. The fatigue crack propagation test and Vickers hardness test of butt weld and base metal were performed. As a result, the fatigue crack propagation test demonstrated a reduced crack propagation rate in both the base metal and the butt weld with a decreasing ambient temperature. For the Vickers hardness, both the welded joint and the base metal at -60℃ presents higher hardness values than RT. Furthermore, the welded joint trends to demonstrates a higher value of Vickers hardness than base metal. Finally, the behavior of fatigue crack propagation in the micro scale between base metal and butt weld at low temperature was described by the fractography.

Keywords: DH36 steel; Vickers hardness; fatigue crack propagation rates; compliance procedures; low temperature.

1. Introduction

With the continuous development of offshore activities in the polar region, the demand of polar ships and offshore structures has considerably increased to operate in the polar environment. Polar ships and offshore structures in polar region has to encounter with the present sea ice, which is the major loads on the structures, and low temperatures, especially the topside structures or open decks of polar ships above the Cold Water Line (CWL), which exposes to the harsh marine environments with extremely cold air below freezing temperatures. The low temperature causes great changes in the mechanical properties of materials and structures, which bring new challenge to the safety operation for polar ships and offshore structures [1].

Polar ships and offshore structures typically experience millions of load cycles during their service under harsh marine environments, which may result in fatigue failure[2]. With the increase in the use of high strength steel material for polar ships and offshore structures, the fatigue of these structures become more serious. Polar ships are prone to fatigue degradation due to the dynamic ice loads mainly caused by ship-ice interaction. Chai and Leira studied the ice loads acting on ship hulls and the fatigue damage resulting from ice loads actions and observed that the fatigue damage due to ice load actions is directly related to the number and distribution of the stress ranges[3]. In the polar environment, the fatigue properties of steels is considerably affected by the

substantial decrease in temperature[4].

The research methods of fatigue are typically divided into the S-N curve method and Fracture Mechanics Method according to the physical integrity of structures [5]. The S-N method is mainly used to evaluate the fatigue crack initiation life of the structure[6], while the fracture mechanics method is mainly used to evaluate the fatigue crack propagation life[7]. The fatigue properties of structures are evaluated by the S-N method in the design phase of the structure. Once the structure is found to have cracks in the service phase, the fracture mechanics method is used to evaluate the fatigue properties of the structure in this state, thereby determining whether the structure needs to be repaired or declare worthless. The purpose of this paper is to provide theoretical support for fatigue properties in the service phase, so the fatigue properties based on fracture mechanics are studied in this paper. In addition, the fracture mechanics approach can be divided into linear elastic fracture mechanics (LEFM) and elastoplastic fracture mechanics (EPFM). The size of the plastic zone is negligible compared to the length of the crack in most polar structures, which is consistent with the conditions of the Linear Elastic Fracture Mechanics Method (LEFM). Therefore, the Linear Elastic Fracture Mechanics Method (LEFM) was used to study the effect of low temperature on fatigue crack propagation rates in this paper.

Based on the Linear Elastic Fracture Mechanics Method (LEFM), a number of design procedures[8-11] have been developed for fatigue-prone structural details to evaluate the fatigue properties of polar ships and other welded steel structures[12, 13]. However, most of these studies only focus on the parameters in the formulation of

Paris's law at RT. The parameters of the Paris formula used in estimating the fatigue life in these design codes derive primarily from the experimental database recorded at RT. Their validity of these parameters at a low ambient temperature requires further validation to enhance fatigue assessment of welded components in polar ships.

Besides, previous investigations have examined experimentally the fatigue crack propagation behavior of structural steels at low temperature, such as Q345qD[14]. Daeho Jeong investigated the fatigue crack propagation behavior of Fe25Mn and Fe16Mn2Al austenitic steels at 298 and 110 K[15]. Jae-Hoon Kim carried out the fatigue crack propagation characteristics of base metal and weld joint of 9% Ni steel for LNG storage tank using CT specimen at RT and -162°C[16]. However, the steel that they studied was not commonly used in polar ships or the temperatures they studied were not suitable for the polar environment. The low temperature fatigue properties of materials that can be applied to polar structural applications remain to be studied in the polar temperature range(-60℃~20℃)[17].

Since DH36 steel is a common steel [17-19] for polar structures, the evaluation of fatigue crack propagation properties for DH36 grade plates plays an important role in the safety of polar structures. DH36 steel is commonly employed on open decks of polar ships, side and transverse bulkheads above CWL, and strength decks other than 0.4 times the length of the ship. The applicable temperature of materials for such components was shown in Table 1[20]. It can be seen that the DH36 steel of these components can cover temperatures of -60°C. A similar specification is given by DNV GL[18]. Therefore, the study of fatigue crack propagation rates of DH36 steel at -60°C

has great practical significance for the evaluation of fatigue properties of polar ships. However, there has been limited research on the fatigue crack propagation rates of DH36 steel in low temperature environment. Therefore, the fatigue crack propagation behavior of DH36 steel and its weld commonly used in polar ships at low temperature remains to be studied.

Table1 Steel grade required for material grade I in low temperature environment

t /mm	Design service temperature (℃)											
	-23~-27℃		-28~-32℃		-33~-38℃		-39~-48℃		-49~58℃		-59~-68℃	
	MS	HT	MS	HT	MS	HT	MS	HT	MS	HT	MS	HT
$t \leq 10$	A	AH	A	AH	B	AH	B	AH	D	DH	D	DH
$10 < t \leq 15$	A	AH	A	AH	B	AH	D	DH	D	DH	D	DH
$15 < t \leq 20$	B	AH	B	AH	B	AH	D	DH	D	DH	E	EH
$20 < t \leq 25$	B	AH	B	AH	D	DH	D	DH	D	DH	E	EH
$25 < t \leq 30$	B	AH	D	DH	D	DH	D	DH	E	EH	E	EH
$30 < t \leq 35$	D	DH	D	DH	D	DH	D	DH	E	EH	E	EH
$35 < t \leq 45$	D	DH	D	DH	D	DH	E	EH	E	EH	-	FH
$45 < t \leq 50$	D	DH	D	DH	E	EH	E	EH	-	EH	-	FH
Where, t is the thickness of steels, MS is Mild steel, HT is High strength steel. The structural steel for hull is divided into general thickness and high strength steel. General strength steel is divided into four grades according to quality: A, B, C and D; high strength steel is divided into two strength grades and three quality grades: AH32, DH32, EH32, AH36, DH36, EH36.												

The fatigue crack propagation behavior can be analyzed by many factors, such as the microstructure, Vickers hardness, and fractography. Some research efforts have studied the effects of Vickers hardness on the fatigue crack propagation under low temperature[21-24]. Such as Chunguo Zhang studied and examined using hardness measurements in conjunction with fatigue crack propagation measurements, he found that Vickers hardness and fatigue crack propagation rates have a close relationship[21]. It is worth noting that all of them found that the hardness has a non-negligible impact on the fatigue crack propagation.

This paper aims to investigate the effect of low temperature on the fatigue crack propagation behavior of the DH36 steel and its butt weld. The tests also try to determine the relationship between the Vickers hardness and fatigue crack propagation behavior. Based on the experimental results, this study attempts to recommend reasonable Paris-law parameters for the fatigue life assessment of cracked welded details under a low ambient temperature. This study firstly describes the testing material and the detailed experimental procedure in Section 2. Section 3 presents the testing results and their data processing. Section 4 discusses the effect of low temperatures on the fatigue crack propagation behavior and compares the fatigue crack propagation properties of the base metal and butt weld. The last section summarizes the primary conclusions drawn from the present study.

2. Fatigue crack propagation test

2.1 Material descriptions

The steel plate used in this test was DH36 steel plate certified by American Bureau of Shipping(ABS). Table 2 shows the chemical compositions of DH36. The typical mechanical properties of DH36 steel were shown in Table 3. The sampling direction was the rolling direction of the steel plate to ensure the same mechanical properties, as shown in Fig. 1(a). The welded plate consists of two pieces of DH36 base steel plates, butt-welded together with a Y-groove through a multi-pass manual flux-cored arc welding process, the groove size is shown in Fig. 1(b). The Welding Procedure is performed according to the welding process of the actual ship. The carbon dioxide arc welding was used for welding, the welding wire is CHE50 and the welding current is

200A, other details refer to Rulers for Material and Welding given by China Classification Society(CCS) [25].

Table 2 Chemical compositions of DH36 steel

	Chemical compositions, %						
	C	Si	Mn	P	S	Als	Cr
DH36	0.17	0.20	1.16	0.018	0.0034	0.023	0.02
	Nb	V	Ti	Mo	Ni	Cu	Ceq
	0.015	0.002	0.017	0	0.01	0.02	0.37

Table 3 The typical mechanical properties of DH36 steel

Temperature	yield strength/MPa	Elastic modulus/GPa	Tensile strength/MPa	Impact energy/J
RT	355.508	206.286	516.072	256.154
-60 deg	431.513	214.883	559.092	64.993

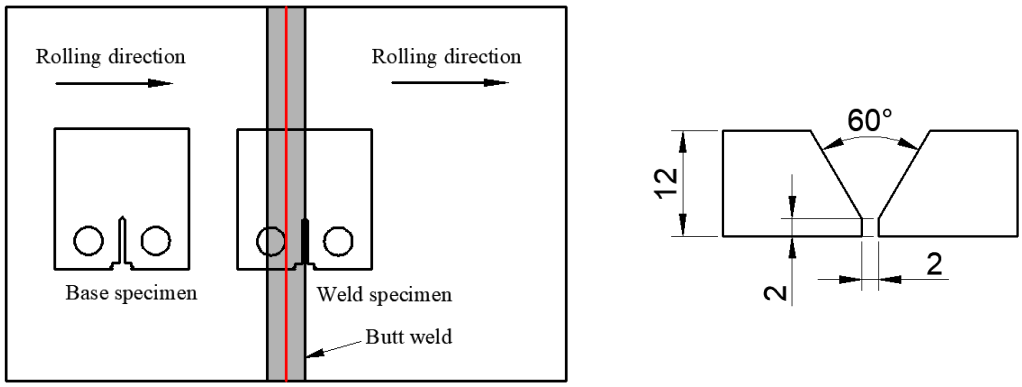

(a)Sampling sketch of the base and weld specimen

(b)The size of groove

Fig. 1 Preparation of specimen

It is worth noting that the butt weld specimen was created such that the crack will initiate at the fusion zone rather than initiating within the weld zone. For polar structures, cracks usually initiate at the weld toe and then propagate along the fusion zone[26]. Therefore, the crack propagation properties of the fusion zone play an important role in the safety of polar structures.

Generally, the fatigue crack propagation behavior with different microstructures is different, so it is necessary to investigate the microstructure of the crack propagation zone. The microstructure of base metal and its butt weld is different[27]. Observations under an optical microscope reveals the microstructures of the base metal and butt weld. The comparison of these materials was shown in Fig. 2.

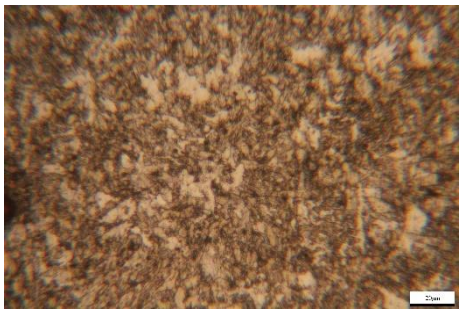

(a)Weld Zone (WZ)

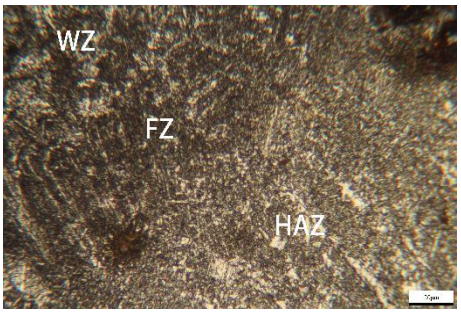

(b)Fusion Zone (FZ)

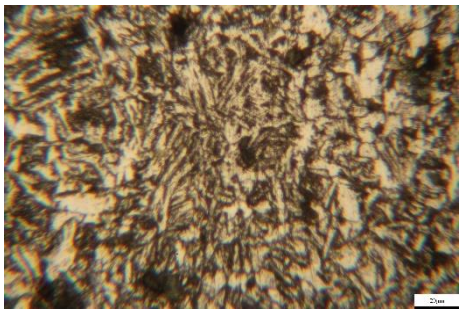

(c)Heat Affected Zone (HAZ)

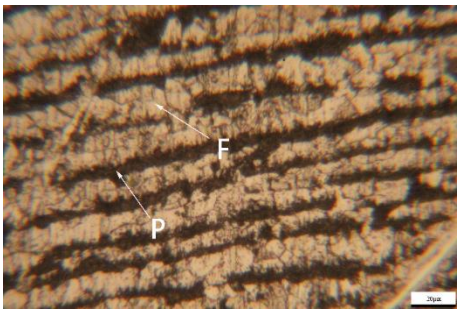

(d)Base Metal (BM)

Fig.2 Microstructures of the investigated DH36 steel and butt weld

In the Weld Zone (WZ), there is a great amount of bainite, and it contains a part of the M/A island. The M/A island consists of martensite and retained austenite[28], as shown in Fig. 2(a).

The Fusion Zone (FZ) is in the transition zone from the weld metal to the base metal in the area close to the weld. The FZ is narrow, with the completely melted weld zone and the completely infusible heat affected zone on both sides, and as shown in Fig.

2(b). The grains in the zone are coarse and the chemical composition and composition are very complex. A certain amount of lath-like martensite exists in the heat affected zone (HAZ), and a part of ferrite staggered, as shown in Fig. 2(c). The zone of the base material (BM) portion is mainly flaky pearlite and quasi-polygonal ferrite, as shown in Fig. 2(d).

2.2 The design of specimens

The size of specimens was referred to the ASTM E647-15. Alvaro and Akselsen simulated butt weld by heating the crack extension zone to 1350 ℃ and then cooling to RT[29]. However, this method of heating did not directly reflect the characteristics of the weld. Therefore, this paper created a real weld on the specimen to study the crack propagation characteristics of the weld. Fig. 3 and Fig. 4 are dimensional drawings of specimens in two forms (base metal, butt weld).

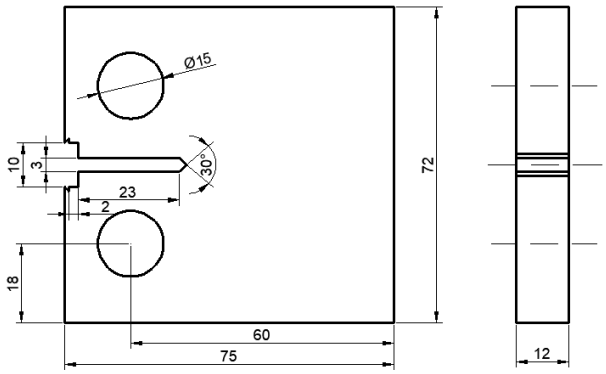

Fig. 3 The specimen of base metal

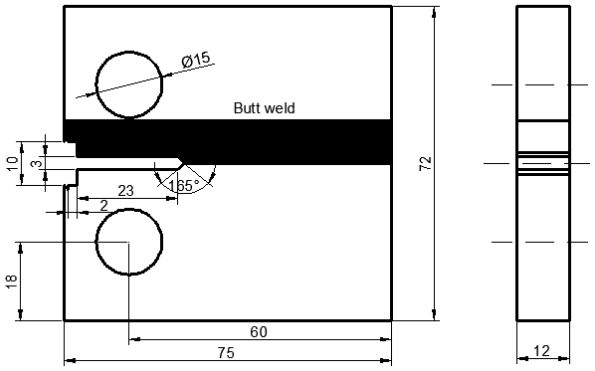

Fig. 4 The specimen of butt weld

There were six specimens for base metal and butt weld, respectively. For the specimen of butt weld, the weld seam needed to be ground away on a grinding machine. As this paper is to study the low temperature crack propagation characteristics of the fusion zone, it is necessary to eliminate the influence of the weld geometric stress concentration. The specimen of butt weld needed to be welded, the two plates need to meet the parallelism requirements, which means the misalignment at any point should be no more than 5% of the thickness, as shown in Fig. 5 [25].

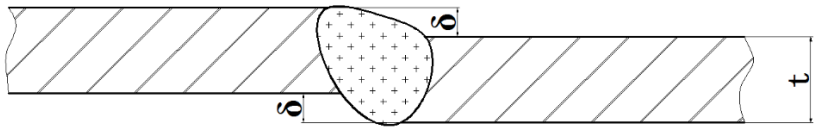

Fig. 5 The Parallelism requirement of the butt weld

2.3 Crack prefabrication

The experimental procedure consisted of a fatigue pre-cracking stage and a crack propagation stage. The fatigue pre-cracking produced a sharp crack tip ahead of the machined notch with a pre-cracking length of approximately 2 to 3 mm. Cracks were prefabricated according to ASTM E647-15. The importance of precracking is to provide

a sharpened fatigue crack of adequate size and straightness which ensures that

1) the effect of the machined starter notch is removed from the specimen *K*-calibration.

2) the effects on subsequent crack growth rate data caused by changing crack front shape or precrack load history are eliminated.

2.4 **Load**

The test was carried out at RT (20℃) and -60℃, the temperature was controlled by a low chamber (Fig. 6(a)), the temperature change was not more than 2℃, and the loading equipment was a PWS-250 fatigue machine. The specimen was rigidly clamped at one end and loaded at the other end, as shown in Fig. 6(b). The peak of loading force was 15kN, the valley value was 1.5kN, the stress ratio *R* was 0.1, the load form was sinusoidal tensile load, and the loading frequency was 10Hz, as shown in Fig. 7.

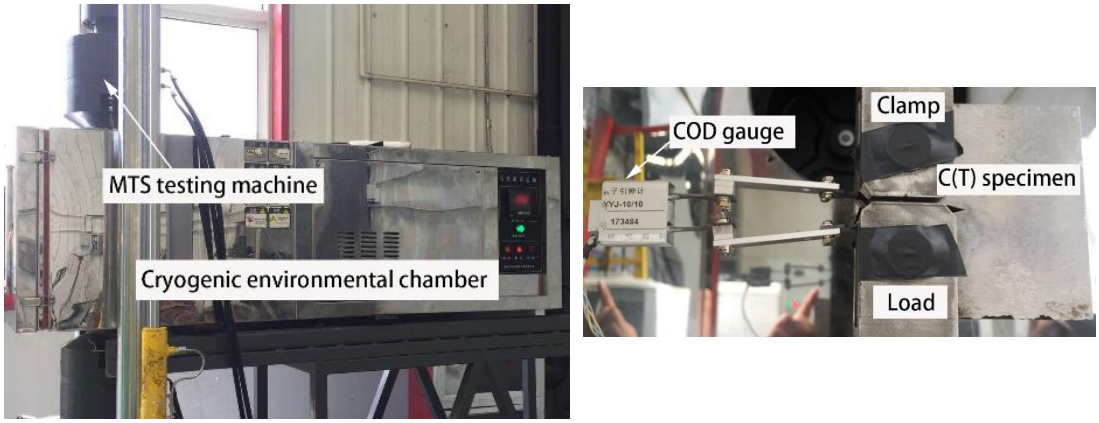

(a)Testing scene (b)Details in the low chamber

Fig. 6 Low temperature experimental setup of fatigue crack propagation test

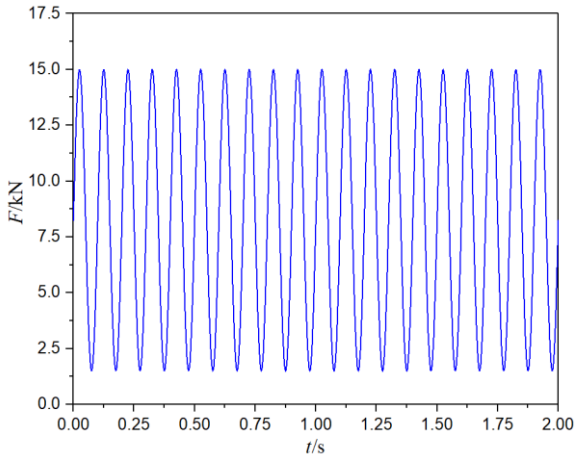

Fig. 7 The loading force

3. Results

In the fatigue crack propagation rate test, the crack length could be determined by the compliance procedures[30]. The test procedure engaged a displacement gauge to monitor the displacement was shown in Fig. 8, which allowed a measurement of the crack size.

$$U_0 = \left\{ \left[\frac{BEV_0}{F} \right]^{1/2} + 1 \right\}^{-1} \tag{1}$$

Where,

U_0 denotes the compliance which is the reciprocal of the force-displacement slope normalized for elastic modulus and specimen thickness,

B denotes the thickness of specimen,

E denotes the elastic modulus,

V_0 denotes the displacement at the measuring point, that is, the displacement measured by the Crack Opening Displacement (COD) gauge.

F denotes the load.

The relationship between compliance and normalized crack length is shown in

equation (2).

$$a/W = 1.001 - 4.6695U_0 + 18.46U_0^2 - 236.82U_0^3 + 1214.9U_0^4 - 2143.6U_0^5 \quad (2)$$

Where,

a denotes the length of crack,

W denotes the width of specimen.

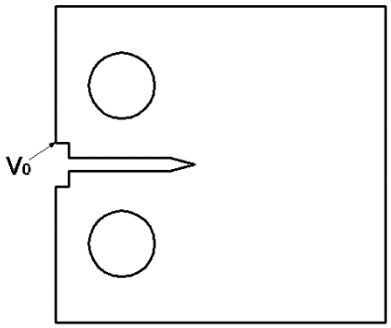

Fig. 8 Compliance measurement position diagram

In order to obtain more stable and accurate results, the relationship of $a-N$ measured by the test is processed by 7-point incremental polynomial method. Paris pointed out that the stress intensity factor ΔK is the main parameter controlling the fatigue crack propagation rate and gives a formula describing the fatigue crack propagation rate[30].

$$da/dN = C(\Delta K)^m \quad (3)$$

$$\Delta K = \frac{\Delta P}{B\sqrt{W}} \cdot \left[(2+\alpha)/(1-\alpha)^{3/2}\right] \cdot (0.886 + 4.64\alpha - 13.32\alpha^2 + 14.72\alpha^3 - 5.6\alpha^4) \quad (4)$$

Where,

a denotes the length of crack,

N denotes cycles,

C , m denotes crack propagation parameters, determined by test,

ΔK denotes the range of stress intensity factor,

ΔP denotes the range of load,

B denotes the thickness of specimen,

W denotes the width of specimen,

α denotes the crack depth ratio a/W .

The above test data was processed by the compliance procedures in ASTM E647-2015. However, the specification does not give a test temperature. Low temperature can cause the changing of mechanical properties such as elastic modulus and yield strength of DH36 steel. It can affect the fatigue crack propagation behavior of DH36 steel. Accordingly, the applicability of the compliance procedures was studied at -60℃, which is the minimum range of temperature that structures can be experienced [17].

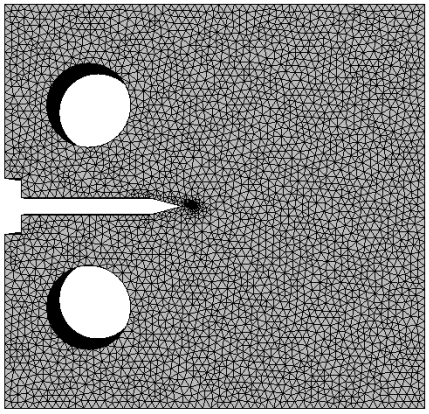

Fig. 9 Finite element model of C(T) specimen

Based on the interactive platform of FRANC 3D and ABAQUS, the fatigue crack propagation behavior of DH36 steel was simulated at RT and -60℃. The specimen used C3D8R reduction elements. The initial crack was introduced in FRANC 3D, and the element type of the crack tip was set to singular elements. The effect of low temperature on the mechanical properties of the material (elastic modulus, yield strength, etc.) was considered. The stress intensity factor of the crack tip evaluated by M-integral.

Knowles and Stemberg [10,11] applied the Nocther's theory to the variational principle and the elastic potential energy principle to propose M-integral. The mathematical explanation for each conservation law is that the integral of a certain function is equal to 0 around the region of the deformation elastic body.

In the case of type I loading:

$$M = \frac{2a(1-\mu^2)}{E} K_{\mathrm{I}}^2 = 2aG_{\mathrm{I}} \tag{5}$$

Where,

M devotes the M- integral,

a devotes the crack length,

μ devotes the Poisson's ratio，

E devotes the elastic modulus,

K_{I} devotes the stress intensity factor,

G_{I} devotes the energy release rate.

What's more, the temperature -60℃ was not applied to the finite element model while calculating the ΔK at -60℃. The finite element model of the C(T) specimen is shown in Fig 9. The results of FEM are plotted in one figure as the $a-V_0$ curve obtained by the compliance procedures, as shown in Fig. 10(a). It can be seen from the Fig. 10(a) that there is a clear difference between the crack length considering the change of the elastic modulus and the crack length without considering the change of the elastic modulus. This means that the crack length a of the C(T) specimen obtained by the compliance procedures should take into account the change in elastic modulus.

Then the accuracy of the ΔK obtained by the compliance procedures was

verified by the compliance procedures, FEM, and theoretical method, as shown in Fig. 10(b). Among them, the theoretical solution of the stress intensity factor of the C(T) sample is as follows,

$$K=\frac{P}{B\sqrt{W}}\left[29.6(\frac{a}{W})^{1/2}-185.5(\frac{a}{W})^{3/2}+655.7(\frac{a}{W})^{5/2}-1017(\frac{a}{W})^{7/2}+639(\frac{a}{W})^{9/2}\right] \quad (6)$$

Where,

K is the stress intensity factor,

P is the load.

It can be seen from Fig. 10(a) that the $a-V_0$ curve obtained by the compliance procedures (without considering the change of elastic modulus), FEM have obvious differences. However, there is no significant difference between the various methods in Fig. 10(b). The difference in the $a-V_0$ curve is caused by the change of elastic modulus. However, ΔK and the elastic modulus are not theoretically directly related. Therefore, ΔK is not affected by the change of elastic modulus.

In summary, as long as the change of the elastic modulus of DH36 steel was considered in this paper, the a and ΔK obtained by the compliance and FEM method can be accurate at RT and -60°C.

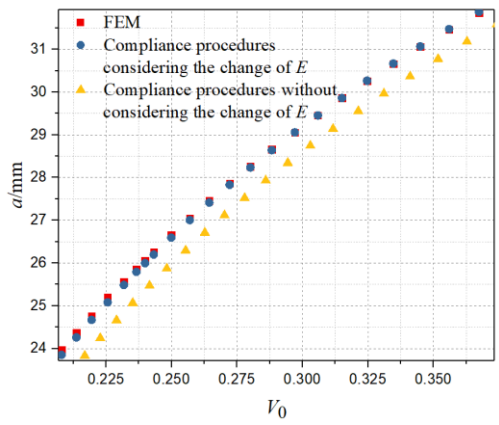

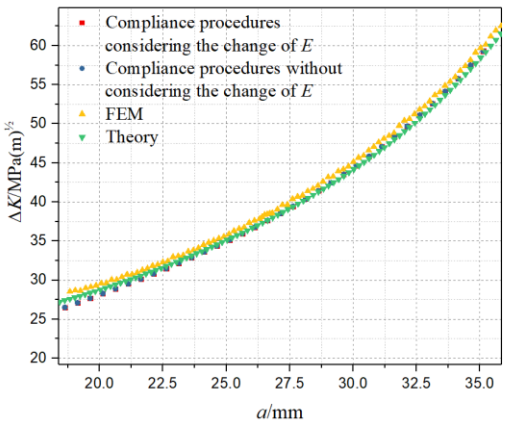

(a) $a - V_0$ (b) $a - \Delta K$

Fig. 10 Verification of the rationality of the compliance procedures

Taking the logarithm of both sides of equation (1) is shown in equation (7)

$$\lg(da/dN) = \lg C + m\lg(\Delta K) \tag{7}$$

It can be seen that $\lg(da/dN)$ and $\lg(\Delta K)$ became a linear relationship, which can be applied with the linear regression on the data by the mean of least squares method in order to estimate *C* and *m* parameters.

Table 4 summarizes the Paris-law parameters *C* and *m* of both materials for the tested stress ratios at different temperatures, which derive from the best fitting curves of the fatigue data. The values of all the correlation coefficient, R^2, of the Paris-law fitting approach exceed 0.9, showing a high level of correlation between the test data and the Paris equation. For the base metal at the stress ratio of $R = 0.1$, with the descent of temperature, the *m* value increases and the *C* value decreases. For the butt weld at stress ratios $R = 0.1$, the same variation in the m and *C* value with respect to the decreasing temperature exists as the base metal at the stress ratios of R=0.1. However, the change in *C* and *m* of butt weld is smaller than that of base metal.

Table 4 Paris-law parameters for the base material and butt weld (ΔK in $\mathrm{MPa}\sqrt{\mathrm{m}}$, da/dN in $\mathrm{mm/cycle}$)

Material	Temperature	P_{max}, KN	*m*	log*C*	R^2
Base metal	RT (20℃)	15	2.333	-7.217	0.983
		15	2.385	-7.262	0.985
		15	2.728	-7.954	0.983
		15	2.647	-7.881	0.993
		15	3.044	-8.601	0.982
		15	2.766	-8.057	0.994
		Mean value	2.651	-7.829	-

		Variance	0.058	0.227	-
	-60℃	15	3.529	-9.531	0.980
		15	3.151	8.731	0.971
		15	3.448	-9.359	0.983
		15	3.274	-9.003	0.970
		15	3.020	-8.480	0.989
		15	3.171	-8.738	0.986
		Mean value	3.266	-6.063	-
		Variance	0.031	43.899	-
Butt weld	RT (20℃)	18	4.676	-11.212	0.963
		18	4.376	-10.637	0.972
		18	3.990	-9.977	0.927
		18	5.461	-12.467	0.960
		18	3.071	-8.329	0.975
		18	4.427	-10.652	0.972
		Mean value	4.334	-10.546	-
		Variance	0.519	1.565	-
	-60℃	15	4.595	-11.278	0.960
		15	4.716	-11.303	0.976
		15	5.496	-12.731	0.924
		15	4.538	-11.027	0.975
		15	4.463	-10.874	0.975
		15	4.345	-10.712	0.988
		Mean value	4.692	-11.321	-
		Variance	0.142	0.441	-

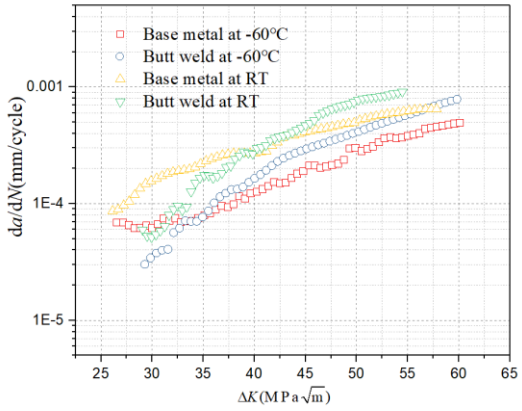

(a) Overview of fatigue crack propagation results

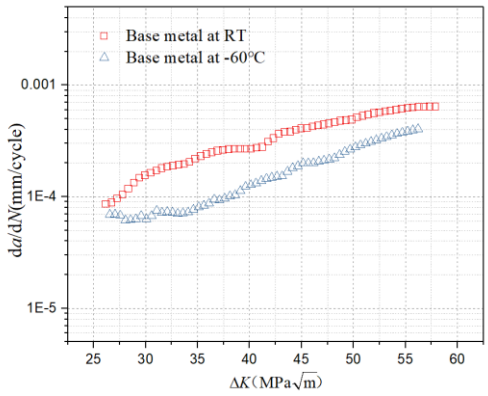

(b)Fatigue crack propagation results for the base metal at -60℃ and RT

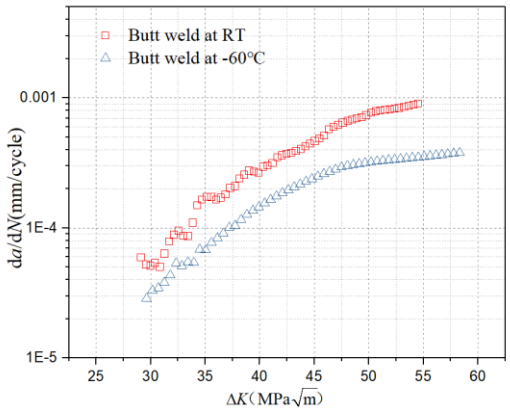

(c)Fatigue crack propagation results for the butt weld at -60℃ and RT

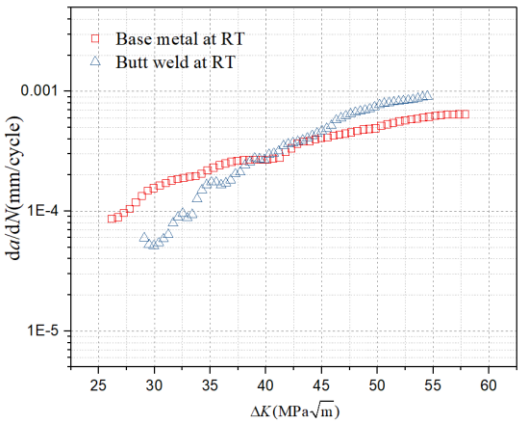

(d)Fatigue crack propagation results for the base metal and butt weld at RT

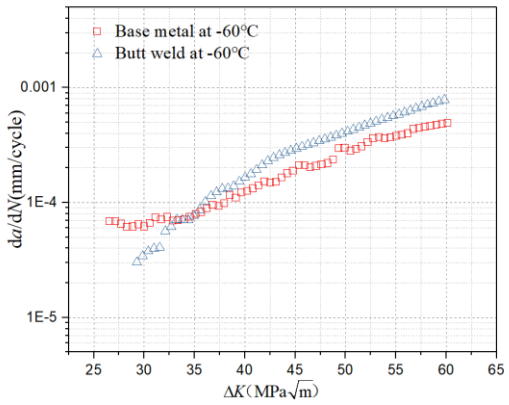

(e)Fatigue crack propagation results for the base metal and butt weld at -60℃

Fig. 11 Fatigue crack propagation results

The six sets of fatigue crack propagation rates curves of base metal and butt weld are converted to the mean fatigue crack propagation rates curves by least squares, respectively. The mean of fatigue crack propagation rates of base metal at RT and -60℃, butt weld at RT and -60℃ are plotted in Fig. 11(a). In general, the crack propagation rate of base metal and butt weld at RT is higher than that of -60 ℃ at the same ΔK.

Fig. 11(b) shows that the mean of fatigue crack propagation rate of the base metal at RT and -60℃. It can be seen that the fatigue crack propagation rate of base metal at RT is 45.396% to 58.644% higher than that of -60℃ at the same ΔK.

For butt weld, the mean fatigue crack propagation rate at RT and -60℃ is demonstrated in Fig. 11(c). propagation rate of fatigue crack for butt weld at RT is about 56.211% to 58.644% higher than that of -60℃ at the same ΔK.

Fig. 11(d) shows the comparison of propagation rate for mean fatigue crack between the base metal and butt weld at RT. The results of base mental represents the higher value of crack propagation rate than butt weld at RT when $\Delta K \leq 40\text{MPa}\sqrt{\text{m}}$. On the other hand, the results demonstrate the opposite trend when the value of stress intensity factor, ΔK higher than 40 $\text{MPa}\sqrt{\text{m}}$. The crack propagation rate of fatigue for the base metal at RT has lower values than butt weld.

The results of mean fatigue crack propagation for the base metal and the butt weld at -60℃ are plotted in the same figure, as illustrated in Fig. 11(e). It can be seen that propagation rate of fatigue crack depends on the value of stress intensity factors ΔK. When $\Delta K \leq 35\text{MPa}\sqrt{\text{m}}$, the fatigue crack propagation rate of the base metal is higher than that the butt weld. Whereas, $\Delta K > 35\text{MPa}\sqrt{\text{m}}$, the fatigue crack propagation rate of the butt weld is higher than the base metal.

4. Discussion

In order to investigated the fatigue crack propagation, the microstructure of crack path should be addressed clearly. The behavior of fatigue crack propagation can be

divided into three stages: the crack initiation stage, the crack stable propagation stage, and the crack instable propagation stage. After the crack initiation, under the action of the alternating load, the main slip surface of the slip band(ie, the direction of the maximum shear stress) extends immediately toward the interior of the metal[31]. Then, the crack enters a stable propagation stage. At this time, the crack propagates in a direction perpendicular to the normal stress stably, and the crack always extends along the fusion zone as shown in Fig. 12. Eventually, the behavior of fatigue crack propagation approaches to the last stage or instable stage, which produces the larger crack size and reduces the cross sectional area of the specimen significantly. This causes a high stress in the sample, and it occurs only a few cycles before the specimen failure. The fatigue crack is propagated along the direction of the maximum shear stress.

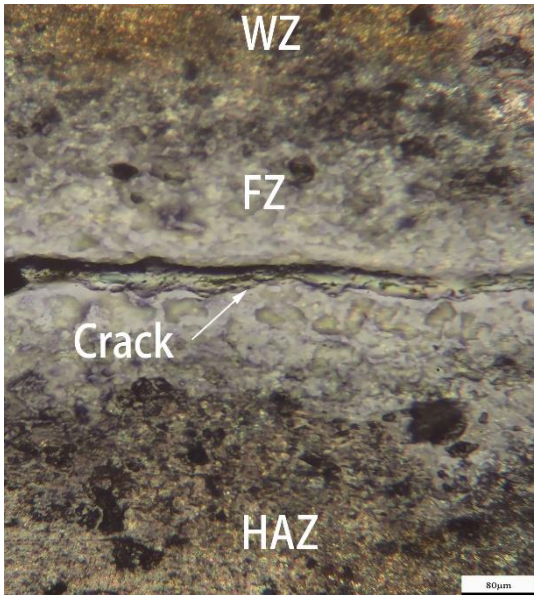

Fig. 12 The path of crack at stable crack propagation stage

Combined with Vickers hardness and fractography, the effect of temperature on the fatigue crack propagation rate of DH36 steel and its butt weld was analyzed in this paper. The crack propagation rate of DH36 steel base metal and its butt weld at the same

temperature was also discussed.

4.1 Low temperature effects

As can be seen from Fig. 11 (a) and (b), the fatigue crack propagation rate of the base metal and the butt weld at RT is higher than -60 °C. In order to analyze the effect of low temperature on fatigue crack propagation behavior, the paper illustrated the Vickers hardness and fractography of base and weld C(T) specimens at RT and -60°C under the stable propagation zone for R = 0.1.

1）Hardness profiles

The Vickers hardness plays an important role in fatigue crack propagation rate[32-34]. Vickers hardness tests were conducted near the fatigue crack propagation path across the BM, HAZ, FZ,WZ of specimen at RT and -60°C. All Vickers hardness were obtained at indentation load of 20 kg-f by using Mitutoyo Hardness Tester (Model AVK-C2). The Vickers hardness profiles are presented in Figs. 13.

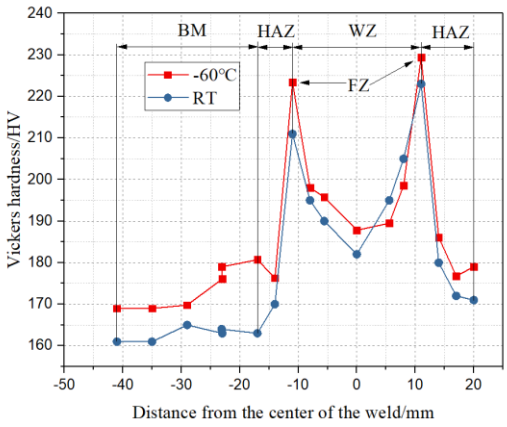

Fig. 13 Vickers hardness profiles across butt weld and base metal at RT and -60°C

As can be seen from Fig. 13, at RT, the Vickers hardness of BM is 161~171HV, the Vickers hardness of HAZ is 170~199 HV, the Vickers hardness of FZ is 211~223

HV, and the Vickers hardness of WZ is 182~205 HV. At -60 ℃, the Vickers hardness of BM is 169~180.7HV, the Vickers hardness of HAZ is 176.3~223.4 HV, the Vickers hardness of FZ is 223.4~229.4 HV, and the Vickers hardness of WZ is 187.8~198.6 HV. The Vickers hardness of the base metal at -60℃ is 17.4 HV higher than that of RT. The Vickers hardness at -60℃ is 12.4 HV higher than that of RT. Combined with Fig. 11 and Fig. 13, it can be found that the discrepancy in Vickers hardness is caused by the different temperature, the relationship between the Vickers hardness and the fatigue crack propagation rate is closely correlated at entire ΔK regime. However, when the discrepancy in Vickers hardness is caused by the different temperature, the relationship between the Vickers hardness and the fatigue crack propagation rate is only correlated at low ΔK regime.

Besides, it is also found that the influence of low temperature on the Vickers hardness of different regions of the welded joint is different. The microstructure of BM is mainly flaky pearlite and quasi-polygonal ferrite, and the Vickers hardness increases from RT to -60℃ by an average of 10.08 HV. The microstructure of HAZ is a lath-like martensite and a small amount of ferrite, and the Vickers hardness changes little from RT to -60℃. The Vickers hardness of FZ increased by an average of 9.4 HV from RT to -60℃. The microstructure of WZ is bainite, and the Vickers hardness at RT to -60℃ is only increased by 0.54 HV. One can find that only the Vickers hardness of BM and FZ is sensitive to low temperatures, which is related to the microstructure inside the area. One can also be considered that the Vickers hardness of flaky pearlite and quasi-polygonal ferrite is sensitive to low temperature, and the Vickers hardness of lath-like

martensite and bainite is not sensitive to low temperature.

2）Fractography

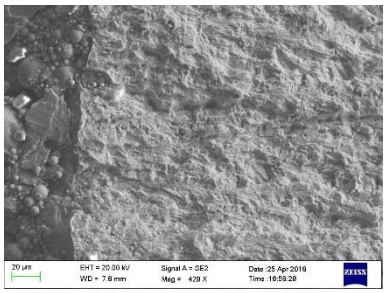

(a) The crack initiation zone of base metal at RT

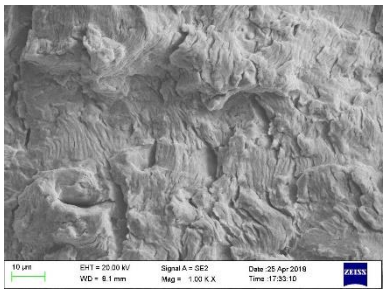

(b)Stable propagation stage of base metal at RT ($\Delta K = 40\text{MPa}\sqrt{\text{m}}$)

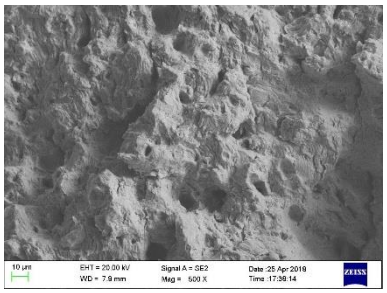

(c)Instable propagation stage of base metal at RT

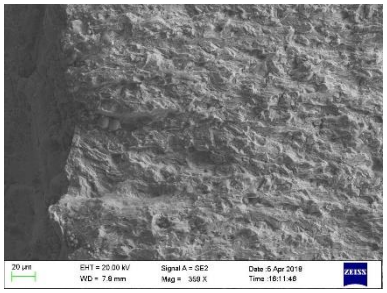

(d) The crack initiation zone of base metal at -60℃

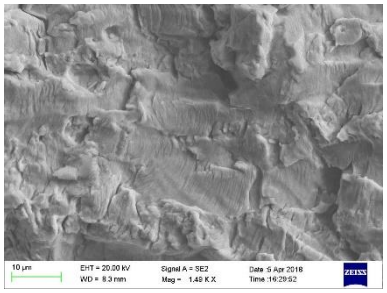

(e) Stable propagation stage of base metal at -60℃ ($\Delta K = 40\text{MPa}\sqrt{\text{m}}$)

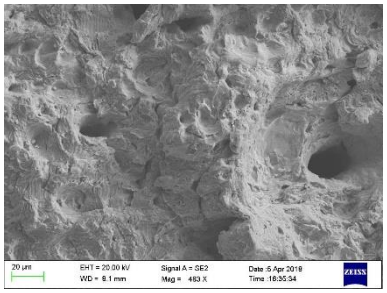

(f)Instable propagation stage of base metal at -60℃

Fig. 14 The fractured surface microstructure for C(T) specimens at RT

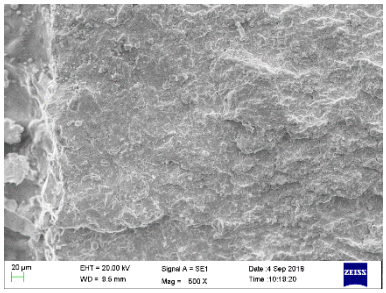

(a) The crack initiation zone of weld at RT

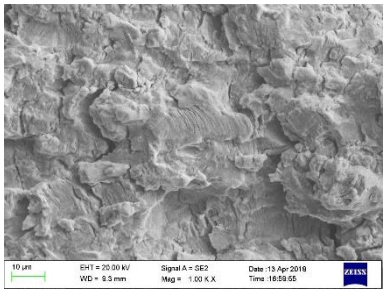

(b) Stable propagation stage of weld at RT ($\Delta K = 40\text{MPa}\sqrt{\text{m}}$)

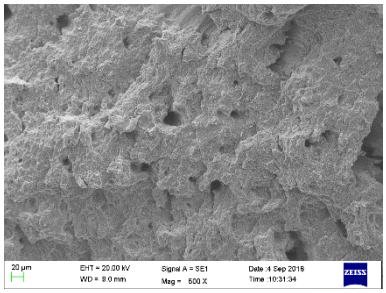

(c)Instable propagation stage of weld at RT

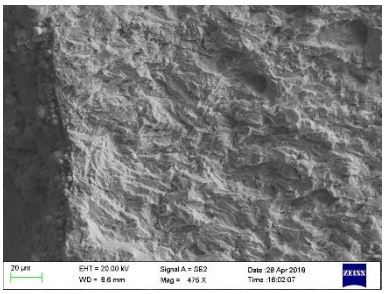

(d) The crack initiation zone of weld at -60℃

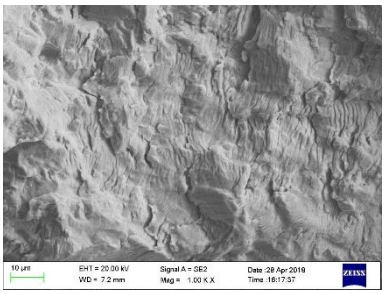

(e)Stable propagation stage of weld at -60℃ ($\Delta K = 40\text{MPa}\sqrt{\text{m}}$)

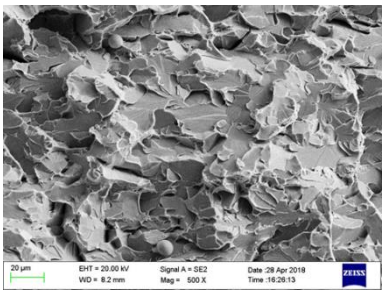

(f)Instable propagation stage of weld at -60℃

Fig. 15 The fractured surface microstructure for C(T) specimens

For base metal specimens, the fracture surface of the crack initiation zone in Fig. 14 (a) and Fig. 14 (d) shows a typical transgranular cleavage surface characterized by a river pattern and a cleavage step. The fracture surface of stable propagation stage in Fig. 14 (b) and Fig. 14 (e), fracture surface at both temperatures have obvious fatigue striations. According to the "plastic passivation model" proposed by Laird and Krause [35], each propagation of the crack has to pass through the process of "opening, passivation, expansion, sharpening". Such a complete process is a stress cycle that leaves a trace on the crack surface called the “fatigue striation”. Therefore, a fatigue striation represents a stress cycle process, and the spacing of the fatigue striations represents the distance corresponding to the crack propagation of the stress cycle, which can reflect the fatigue crack propagation rate[36]. The spacing of fatigue striations at the RT is wider than that of -60℃, which reflects the fatigue crack propagation rate of the base metal at RT is higher than that of -60℃. The fracture surface of instantaneous fracture zone in Fig. 14 (c) and Fig. 14 (f), the fractures have obvious dimples at the two temperatures, and the fracture states in this region are plastic fractures. Therefore, there is no remarkable morphological difference between base metal at RT and -60℃

in the fracture mode.

For butt weld specimens, the fracture surface (Fig. 15 (a) and Fig. 15 (d)) of the crack initiation zone at the RT features the transgranular quasi-cleavage facet with a mixture of short river pattern, small cleavage plane, and tearing ridge, while the fractographs at -60℃ exhibit cleavage fracture with river patterns and cleavage steps. The fracture surface of the stable propagation stage in Fig. 15 (b) and Fig. 15 (e), the spacing of fatigue striations at the RT is wider than that of -60℃, which reflects the fatigue crack propagation rate of the butt metal at RT is higher than -60℃. The fracture surface of instantaneous fracture zone in Fig. 15 (c) and Fig. 15 (f), The cleavage step of the butt weld fracture at RT coexists with the dimple, which is a mixed fracture. The fracture at -60°C presents a fan-shaped cleavage river pattern. At low temperatures, when the difference in orientation between adjacent grains is large, the cleavage cracks along the expansion direction to the grain boundary and impacts the grain boundary, and nucleates in the next grain, and expands outward in the shape of a fan. A fan-shaped cleavage fracture is formed[37]. This implies the fracture mode has shifted from quasi-cleavage to cleavage as the temperature decreases from the RT to -60℃.

The Vickers hardness at -60℃ is higher than that of RT, the fatigue crack propagation rate of DH36 steel base metal and butt weld at -60℃ is lower than that of RT, and the spacing of fatigue fringes on the fracture at -60℃ is also smaller than that of RT at entire ΔK . It can be found that the Vickers hardness, fatigue crack propagation rates and fatigue fracture surface characterizations are closely correlated at low ΔK regime. These results of base metal are in agreement with the conclusions reported by

X.W. Liao, but results of butt weld are opposite to conclusion reported by him[14]. The resistance against fatigue crack propagation of the butt weld increases at a decreasing ambient temperature in this paper, while the fatigue crack propagation rate of butt weld accelerates at the low ambient temperature in his research. This is because the crack tip he studied is located on the center line of the butt weld, and the crack spreads on this center line. The area where this center line is located at WZ. The crack tip of this paper is located at the boundary line between the butt weld and the base metal, and the crack extends along this boundary line which is located at FZ. In the study of X.W. Liao, the microstructure of the WZ is a mixture of bainite, acicular ferrite, and a little perlite, which leads to satisfactory low-temperature toughness. In this paper, the microstructure of the FZ is very complex with coarse grains. The mechanical properties of FZ are weak in welded joints, which largely determine the properties of welded joints. It can be seen that the FZ in this paper and WZ in study of X.W. Liao have different microstructure and mechanical properties, their crack propagation performance is also very different.

4.2 Comparison of fatigue crack propagation behavior between base metal and butt weld

1）Discussion of results with Vickers hardness measurements

The Vickers hardness of the FZ is 62 HV higher than that of the BM at RT, and the Vickers hardness of the FZ is 68.4 HV higher than that of the BM at -60℃ (Fig. 12).

Combining Fig. 12 and Fig. 10(a), Fig. 10(b), it is worth noting that the fatigue crack propagation rate increases with the Vickers hardness decreases at low ΔK

regime. But as ΔK increases, this relationship is no longer maintained. This can attribute to the micro-failure mode in the low expansion rate region is single shear, and the influence of the microstructure property is large, so the hardness of the material has a great influence on it. In the stable propagation stage, its micro-failure mode is the striated or double-slip mode, and the influence of microstructure performance is small, so the hardness of the material has little influence on it. In the instantaneous fracture zone, its micro-failure mode is the additional static mode, the fatigue crack propagation rate at this time is quite sensitive to hardness. However, the fatigue crack propagation rates at this stage is so large that the effect of hardness is not significant[38].

The fatigue crack propagation rates of base metal and butt weld tend to decrease with decreasing temperature due to different mechanisms. Other than the Vickers hardness, residual stress and a variety of metallurgical factors, including grain size and phase transformation, may affect the fatigue crack propagation behavior of the welds, which further complicates the understanding on the fatigue crack propagation behavior of the welds. Because of such difficulties, the fatigue crack propagation studies on steel welds are extremely limited despite the practical importance. In order to understand the effect of microstructure of DH36 steel and its butt weld on fatigue crack propagation behavior, optical micrographic observation was conducted. Combined with Fig. 2 (b) and (d), it can be seen that the microstructure of both zones is absolutely different. The grains in FZ are coarse, the chemical composition and composition in FZ are very complex (Fig. 2(b)). The microstructure of the BM is mainly flaky pearlite and quasi-polygonal ferrite (Fig. 2(d)).

2）Discussion of results with the analysis of the fracture surfaces

There is no remarkable morphological difference between base metal and butt weld at RT in the fracture mode. At -60℃, the fracture surface of the stable propagation stage is shown in Fig. 14 (e) and Fig. 15 (e), the spacing of fatigue striations of butt weld is wider than that of base metal at -60℃, which reflects the fatigue crack propagation rate of the butt weld is higher than base metal at -60℃. The fracture surface of instantaneous fracture zone is shown in Fig. 14 (f) and Fig. 15 (f), the cleavage step of the butt weld fracture at RT coexists with the dimple, which is a mixed fracture. The fracture at -60 °C presents a fan-shaped cleavage river pattern.

5. Conclusions

This paper investigated the fatigue crack propagation behavior of DH36 base metal and its butt weld by fatigue crack propagation tests and Vickers hardness tests at RT and -60℃. The above investigation leads to the following conclusions,

(1) The compliance procedures in the specification is still suitable at -60℃, but the effect of low temperature on the elastic modulus of the material must be considered.

(2) The presence of low temperature causes a decrease in the fatigue crack propagation rate of the base metal and weld fusion zone. At -60℃, the fatigue crack propagation rate at the weld fusion zone is higher than that of the base metal.

(3) Vickers hardness has a significant effect on crack propagation rate only at low ΔK, but Vickers hardness may have insignificant effects on crack propagation rate at high ΔK.

(4) For ship structures that are exposed to -60℃, the anti-fatigue design of these ship structures can refer to the fatigue crack growth rate at -60℃. Similarly, for ship structures that are exposed to room temperature, the anti-fatigue design of these ship structures can refer to the fatigue crack growth rate at room temperature.

Acknowledgement

This paper was supported by the National Natural Science Foundation of China, Fund No. 51679050.

Reference

[1] W. Zhao, J. Cao, G. Feng, H. Ren, Investigation on Temperature Dependence of Yielding Strength for Marine DH36 Steel, Shipbuilding of China, 59 (2018) 108-115.
[2] W. Fricke, A. von Lilienfeld-Toal, H. Paetzold, Fatigue strength investigations of welded details of stiffened plate structures in steel ships, International Journal of Fatigue, 34 (2012) 17-26.
[3] W. Chai, B.J. Leira, A. Naess, Short-term extreme ice loads prediction and fatigue damage evaluation for an icebreaker, Ships and Offshore Structures, 13 (2018) 127-137.
[4] X. Yan, X. Huang, Y. Huang, W. Cui, Prediction of fatigue crack growth in a ship detail under wave-induced loading, Ocean Engineering, 113 (2016) 246-254.
[5] U. Krupp, Fatigue crack propagation in metals and alloys, 10 (2007) 53.
[6] H.J. Nolte K, Closed-form expressions for determining the fatigue damage of structures due to ocean waves, in: Proceedings Offshore Technology Conference, 1976, pp. 861-870.
[7] E.F. Paris P, A Critical Analysis of Crack Propagation Laws, 85 (1963) 528-533.
[8] J.P. Hsu, D. Wang, H. Kahn, F. Ernst, G.M. Michal, A.H. Heuer, Fatigue crack growth in interstitially hardened AISI 316L stainless steel, International Journal of Fatigue, 47 (2013) 100-105.

[9] B.L. Josefson, J.W. Ringsberg, Assessment of uncertainties in life prediction of fatigue crack initiation and propagation in welded rails, International Journal of Fatigue, 31 (2009) 1413-1421.

[10] K. Kiss, L. Dunai, Fracture mechanics based fatigue analysis of steel bridge decks by two-level cracked models, Computers & Structures, 80 (2002) 2321-2331.

[11] A. Pipinato, C. Pellegrino, C. Modena, Fatigue assessment of highway steel bridges in presence of seismic loading, Engineering Structures, 33 (2011) 202-209.

[12] C. Albuquerque, A.L.L. Silva, A.M.P. de Jesus, R. Calçada, An efficient methodology for fatigue damage assessment of bridge details using modal superposition of stress intensity factors, International Journal of Fatigue, 81 (2015) 61-77.

[13] X. Qian, C.T. Nguyen, Y. Petchdemaneengam, Z. Ou, S. Swaddiwudhipong, P. Marshall, Fatigue performance of tubular X-joints with PJP+ welds: II — Numerical investigation, Journal of Constructional Steel Research, 89 (2013) 252-261.

[14] X.W. Liao, Y.Q. Wang, X.D. Qian, Y.J. Shi, Fatigue crack propagation for Q345qD bridge steel and its butt welds at low temperatures, Fatigue & Fracture of Engineering Materials & Structures, 41 (2018) 675-687.

[15] D. Jeong, H. Sung, T. Park, J. Lee, S. Kim, Fatigue crack propagation behavior of Fe25Mn and Fe16Mn2Al steels at room and cryogenic temperatures, Metals and Materials International, 22 (2016) 601-608.

[16] K.-T.S. Jae-Hoon Kim, Young-Kyun Kim and Byoung-Wook Ahn, Fatigue Crack Growth Characteristics of 9% Ni Steel Welded Joint for LNG Storage Tank at Low Temperature, (2010).

[17] ABS, Rules for Building and Classing Steel vessels, in, 2019.

[18] DNVGL, Rules for Classification of ships new building, in, 2017.

[19] CCS, Rules and regulations for the construction and classification of sea-going steel ships, in: 8, 2018.

[20] CCS, Rules for Classification of Sea-Going Steel Ships, in, 2018.

[21] C. Zhang, X. Hu, P. Lu, Fatigue and hardness effects of a thin buffer layer on the heat affected zone of a weld repaired Bisplate80, Journal of Materials Processing

Technology, 212 (2012) 393-401.
[22] A. Casagrande, G.P. Cammarota, L. Micele, Relationship between fatigue limit and Vickers hardness in steels, Materials Science and Engineering: A, 528 (2011) 3468-3473.
[23] J. Li, Y. Shi, X. Wu, Effect of initial hardness on the thermal fatigue behavior of AISI H13 steel by experimental sand numerical investigations, Fatigue & Fracture of Engineering Materials & Structures, 41 (2018) 1260-1274.
[24] M.D. Chapetti, Hardness as a tool for the estimation of the microstructural threshold, Procedia Structural Integrity (2017) 229-234.
[25] CCS, Rulers for Material and Welding, in, IACS, 2018.
[26] Y. Xiong, X.X. Hu, The effect of microstructures on fatigue crack growth in Q345 steel welded joint, Fatigue & Fracture of Engineering Materials & Structures, 35 (2012) 500-512.
[27] H. Yuan, W. Zhang, G.M. Castelluccio, J. Kim, Y. Liu, Microstructure-sensitive estimation of small fatigue crack growth in bridge steel welds, International Journal of Fatigue, 112 (2018) 183-197.
[28] L. Lan, C. Qiu, D. Zhao, X. Gao, L. Du, Microstructural characteristics and toughness of the simulated coarse grained heat affected zone of high strength low carbon bainitic steel, Materials Science and Engineering: A, 529 (2011) 192-200.
[29] O.M.A. Antonio Alvaro, Xiaobo Ren, Alexander Kane, Fatigue Properties of a 420 MPa Structural Steel at Low Temperature, in: Proceedings of the Twenty-fifth (2015) International Ocean and Polar Engineering Conference, Kona, Big Island, Hawaii, USA, 2015.
[30] ASTM, Standard test method for measurement of fatigue crack propagation rates, in, 2015.
[31] L. Eisenhut, F. Schaefer, P. Gruenewald, L. Weiter, M. Marx, C.J.I.J.o.F. Motz, Effect of a dislocation pile-up at the neutral axis on trans-crystalline crack growth for micro-bending fatigue, 94 (2017) 131-139.
[32] R. Cortés, N.K. Rodríguez, R.R. Ambriz, V.H. López, A. Ruiz, D. Jaramillo, Fatigue and crack growth behavior of Inconel 718–AL6XN dissimilar welds, Materials

Science and Engineering: A, 745 (2019) 20-30.

[33] C. Zhang, S. van der Vyver, X. Hu, P. Lu, Fatigue crack growth behavior in weld-repaired high-strength low-alloy steel, Engineering Fracture Mechanics, 78 (2011) 1862-1875.

[34] A.A. Shaniavskiy, A.L.J.E.F.A. Toushentsov, Mechanisms of fatigue crack initiation and propagation in cast aluminum alloy AL5 of hydropumps NP-89D in aircraft Tu-154M, 17 (2010) 658-663.

[35] C. Laird, A.R. Krause, A theory of crack nucleation in high strain fatigue, International Journal of Fracture, 4 (1968) 219-231.

[36] V. Richter-Trummer, R.M.C.Miranda, C. Albuquerque, Fatigue Crack Striation Spacing for Welded and Base Material CT Steel Specimens, ADVANCED MATERIALS FORUM VI, PTS 1 AND 2, 730-732 (2013) 793.

[37] T.S. Srivatsan, M.A. Imam, R. Srinivasan, Fatigue of Materials, Cambridge University Press, 1991.

[38] V. Landersheim, M. Jöckel, C.E. Dsoki, T. Bruder, H.J.I.J.o.F. Hanselka, Fatigue strength evaluation of linear flow split profile sections based on hardness distribution, 39 (2012) 61-67.